JOURNAL OF CATALYSIS 146, 422–436 (1994)

Elementary Steps in CO Hydrogenation on Rh Catalysts Supported on ZrO_2 and Mo/ZrO_2

E. Guglielminotti*, E. Giamello*, F. Pinna†, G. Strukul†, S. Martinengo‡, and L. Zanderighi§

*Dipartimento di Chimica Inorganica, Chimica Fisica e dei Materiali, Università di Torino, Via P. Giuria 7, 10125 Torino, Italy; †Dipartimento di Chimica, Università di Venezia, Dorsoduro 2137, 30123 Venezia, Italy; ‡Dipartimento di Chimica Inorganica e Metallorganica, e Centro CNR sui bassi Stati di Ossidazione, Università di Milano, Via G. Venezian 21, 20133 Milano, Italy; and §Dipartimento di Chimica Fisica ed Elettrochimica, Università di Milano, Via Golgi 19, 20133 Milano, Italy

Received January 4, 1993; revised July 3, 1993

The first steps of CO activation and hydrogenation reactions on Rh catalysts have been studied in order to identify possible intermediates in the reaction pathway to C_1 compounds. Rh catalysts were prepared by supporting $Rh_4(CO)_{12}$ on ZrO_2 or on ZrO_2 after adsorption of $Mo(CO)_6$. The Rh content on all catalysts was 1% (w/w) while the Mo/Rh atomic ratio ranged from 0.0 to 2.0. The supported catalysts were decomposed in H_2 at 523 K (LTR) and at 773 K (HTR). The samples were characterized by TEM, EPR, FTIR, and chemisorption of H_2, O_2, and CO. The catalytic activity was tested in the CO hydrogenation reaction at 493 K and 101 kPa. After the thermal treatment Mo was present on the surface as Mo(V) and Mo(VI). The total CO conversion increased with Mo/Rh ratio on LTR catalysts while it was unaffected on HTR catalysts. By increasing the Mo content the amount of CO_2 formed increased significantly. The CO carbon efficiency to methane and total hydrocarbon without CO_2, did not depend on the Mo/Rh ratio for LTR catalysts while a constant decrease was observed for HTR catalysts. The carbon efficiency to methanol increased with the Mo content both on LTR and HTR catalysts, and that to ethanol changed with the Mo/Rh ratio and the activation temperature. Mo and Rh form a very complex interacting system: Mo inhibits the sintering of highly dispersed Rh obtained by $Rh_4(CO)_{12}$ decomposition, and in the presence of hydrogen Rh promotes the reduction of MoO_3 with the formation of Mo bronzes. The environment of Rh particles is strongly modified by the presence of Mo as evidenced by modification of the IR spectrum of chemisorbed CO both in the linear and in the bridged Rh–CO region. On the basis of the experimental results the reaction paths to CO_2, CH_3OH, and CH_4, and the effect of MoO_3 promoter are discussed in detail. The methane formation through different pathways involving a bicarbonate and/or a formate intermediate are presented.

INTRODUCTION

The ability of rhodium catalysts to produce ethanol as well as a variety of other substances such as methanol, hydrocarbons, higher alcohols, acetaldehyde, and acetic acid in carbon monoxide hydrogenation has been known since 1978 (1). The activity and selectivity of rhodium catalysts are influenced greatly by many parameters, including the support and/or promoters used, the precursors and the preparation techniques, and, to a lesser extent, by the reaction experimental conditions (2). On Rh/SiO_2 catalysts methane and higher hydrocarbons are the main products, and little or no ethanol is observed (3), while on Rh/CeO_2 catalysts ethanol is the main product with up to 80% selectivity (4).

A large number of metallic oxides have been used either as supports or as promoters, and an analysis of some of the topics concerned has been presented recently by Ponec (5). According to Sachtler and Ichikawa (6) oxidic promoters can be classified in at least two distinct groups:

(a) "oxophilic" metal oxides which enhance the CO dissociation rate and therefore also the steady-state coverage of the surface with alkyl groups. They also appear to stabilize acyl species which are the precursors for C_2-oxygenates. As a result CO conversion is increased while the selectivity to oxygenates is high.

(b) "basic" metal ions which block the large Rh ensembles required for CO dissociation and substantially suppress the CO_2 formation. Their presence therefore results in a depression of methanation and in a promoted CO insertion favoured by Rh isolated sites on the surface.

Carbon monoxide hydrogenation might appear to be a simple reaction easy to describe mechanistically. However, only the reaction mechanisms for methanol formation on metallic oxides (7) and methane or higher hydrocarbon formation on metallic surfaces (8), have been highlighted in recent years. As the spectrum of products becomes larger a multiplicity of reaction paths can occur: the reaction mechanisms proposed for the formation of any given product are numerous and not consistent with each other. A typical case is the pathway for ethanol formation for which some authors suggest a direct reaction from CO/H_2 (8–12), while others propose hydrogena-

0021-9517/94 $6.00

tion of acetaldehyde (4, 13–15), considered as an intermediate species.

To simplify the study of the CO reaction mechanism we have concentrated our interest on the first steps of CO activation and reaction in order to identify some possible intermediates in the reaction path to C_1 compounds. This knowledge is preliminary to the study of the path to ethanol or longer chain compounds.

Most authors agree that CO dissociation is impossible or very slow on a flat surface such as f.c.c. Rh(111), while at steps and kinks, that is on a rough surface, CO seems to dissociate even at low temperature (16, 17). Thus CO dissociation is a structure-sensitive reaction. On metallic Rh only hydrocarbons are formed in the CO hydrogenation reaction but when the surface has been oxidized also oxygenated compounds are formed (18).

The description of the reaction path becomes complicated when supported Rh is considered. The CO dissociation must depend on the Rh ensemble, but the interaction between CO molecules and Rh is influenced by the presence of the support. The effect of the support can be both of a physical nature, such as to change the electron density on the metal particle or the polarization of the adsorbed CO, and of a chemical nature, due to its interaction with the oxygen end of CO chemisorbed on Rh (5). It is at this level that the chemical nature of the promoters plays some role.

Here we study the CO activation and its reactivity on Rh/ZrO_2 and $Rh–Mo/ZrO_2$ catalysts. For this purpose we have prepared the Rh catalysts by supporting $Rh_4(CO)_{12}$ on ZrO_2, and on ZrO_2 with preadsorbed $Mo(CO)_6$. The carbonyls were decomposed in a hydrogen stream at two different temperatures. All catalysts were characterized by TEM, to obtain information on surface morphology, EPR, to identify possible paramagnetic species present in the catalyst, FTIR with probe molecules, to characterize surface CO intermediates, and H_2 and O_2 chemisorption and TPR to highlight the role of the promoter and of the thermal treatment. The catalysts were also characterized by activity and selectivity measurements in a flow reactor.

EXPERIMENTAL

Zirconium oxide was prepared by dropping a 28% ammonia solution into an aqueous solution of $ZrOCl_2 \cdot 8H_2O$ (Riedel) with stirring. After filtration, the precipitated zirconium hydroxide was placed into a slightly warm ammonia solution (pH = 8–9) and washed with stirring; filtration and washing were repeated until disappearance of the chloride ions ($AgNO_3$ test). The precipitate was dried in an oven at 388 K for 15 h, then heated at 773 K (5 K/min) in a fluidized bed oven and calcined for 2 h in a stream of air (2.4 liter/h).

Catalysts were prepared in inert atmosphere, adding a solution of $Mo(CO)_6$ (Fluka) in *n*-heptane to a suspension of ZrO_2. At room temperature (RT) the adsorption of the carbonyl was only partial, and was completed by heating under reflux until the solution showed no $Mo(CO)_6$ IR bands. A heptane solution of $Rh_4(CO)_{12}$ (19) was then added at RT, and the suspension was stirred until complete adsorption. The Rh content for all samples was 1.0% w/w, while the Mo/Rh atomic ratio changed from 0.0 to 2.0 (0/1; 0.25/1; 0.5/1; 0.75/1; 1/1; 2/1). Supported carbonyls decomposed in H_2 at 523 K (LTR samples) and 773 K (HTR samples) were passivated with 5% O_2 in Ar at 298 K. The resulting catalysts were stored in air.

The TEM experiments on HTR samples were performed with a Jeol 2000 EX electron microscope working at high resolution (600,000 magnification, at 200 kV) and equipped with a top entry stage.

A Varian E-109 spectrometer operating in the X-band mode and equipped with a dual cavity was used for the EPR spectra. Varian pitch was used for g-value calibration.

The FTIR spectra were recorded at RT with a Perkin–Elmer 1760 spectrometer. The passivated samples were reduced *in situ* in static conditions at 523 or 773 K, changing the H_2 during the reduction and with a final outgassing at the same temperature to remove the adsorbed water. High purity gases (>99.9% H_2, CO, CO_2, and O_2 from Matheson) were utilized without further purification.

H_2 and O_2 chemisorptions were performed at 298 K using a pulse flow technique (0.98 cm^3 per pulse). Before measurements, catalysts were heated (10 K/min) in a H_2 stream (5% in Ar, flow rate 40 ml/min) at 523 K (LTR) or 773 K (HTR), and then for 2 h in a stream of pure H_2. After reduction the surface was cleaned for 3 h with an Ar stream, then cooled at 298 K, always in Ar flow. The chemisorption measurements were performed with 5% diluted H_2, O_2 in Ar, and CO in He by a sampling valve with calibrated capillary (0.96 ml). Before use H_2, CO, and Ar were purified by an Oxy-trap (Alltech). In the TPR experiments all samples were calcined at 773 K for 1 h in an oxidizing flow (5% O_2 in Ar), cooled to 298 K, treated with pure Ar, and then reduced by heating (10 K/min) to 1023 K in a 5% H_2 in Ar mixture.

Catalytic activity was studied in a glass flow reactor (i.d. 8 mm, length 200 mm) at 493 K, 101 kPa, H_2/CO = 3/1. Before testing, the catalysts were activated *in situ* at 523 K (LTR) or 773 K (HTR) in H_2 flow for 2 h. The catalyst used, 1.2 g, was diluted with carborundum to avoid temperature gradients; in order to have low CO conversion (<10%) the feed flow rate was adjusted for low contact time (τ = 0.06 g min/ml). The reacted mixture was analyzed by an on-line G.C.

RESULTS

The prepared ZrO_2 had a BET surface area of 70 m^2/g; x-ray analysis showed 87% monoclinic and 13% tetragonal structure.

(*a*) *TEM.* Micrographs were obtained for Rh/ZrO_2 and Mo/Rh = 2 HTR samples, exposed to the atmosphere before being introduced into the vacuum chamber of the microscope. By comparing the distances measured for the interference fringes of the micrographs with the more intense diffraction peaks of (*hkl*) lattice planes, the ZrO_2 crystals (dimension 10–20 nm) were found to be monoclinic (JCPDS Tables 36–420, monoclinic ZrO_2, d = 3.163 Å, [111] plane), together with a minor amount of ZrO_2 tetragonal phase. Besides, only clear evidence was found of particles of 3-nm Rh_2O_3 microcrystals (JCPDS, 25–707, d = 3.68 Å, [012] plane) on Rh/ZrO_2 samples and of a slightly reduced Mo_9O_{26} Magnéli phase (JCPDS 12–1753, d = 3.366 Å, [033] plane) on Mo/Rh = 2 HTR sample. The possible presence of $Zr(MoO_4)_2$ phase (JCPDS 38–1466, d = 3.834 Å, [112] plane) cannot be confirmed for the error, >0.1 Å, due to the very small dimension of the microcrystals.

(*b*) *EPR spectra.* The Rh/ZrO_2 sample, after outgassing, exhibited two signals whose intensity remained constant even after reduction in hydrogen at 523 K and 773 K, respectively (spectrum not reported for sake of brevity). The first signal was a narrow line around the free spin resonance value (g = 2.0023) which could be due to some impurities (the sample contained about 0.001% Fe) or, more likely, to a paramagnetic defect of the matrix. The second weak and scarcely resolved signal was observed at higher field. The signal had the features of the resonance of a d^1 ion, and it could be attributed to partially reduced species, either Zr^{3+} ions (20) or Ti^{3+} ions since traces of Ti were present in the sample as impurities. The presence of paramagnetic Rh^{2+} ions on this sample may be excluded.

The Mo/Rh = 0.25 sample outgassed at 523 K exhibited the typical EPR spectrum of the Mo(V) ion (Fig. 1). Mo(V) is a $4d^1$ ion whose resonance occurs at g values lower than the free spin value. The spectrum also has hyperfine structure due to the interaction of the unpaired electron with the ^{95}Mo and ^{97}Mo nuclei whose abundance is 25%. This ion has been observed in the past at the surface of many molybdenum-containing heterogeneous systems (21, 22). The spectrum in Fig. 1 is characterized by the presence of two distinct species (both with axial symmetry of the g tensor) with slightly different spin-hamiltonian parameters. The former one (species A) exhibits the following values: $g_\parallel$ = 1.896, $g_\perp$ = 1.960, A = 55 G and the second one (species B), slightly less abundant, $g_\parallel$ = 1.864,

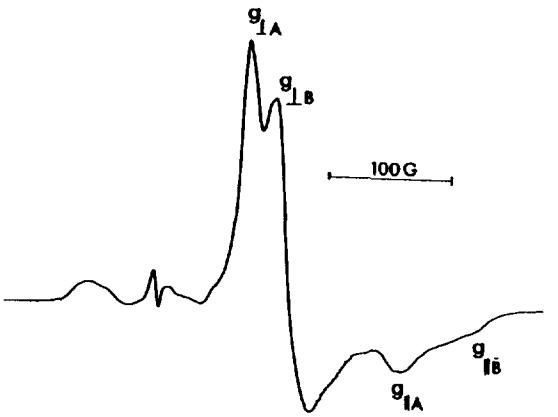

FIG. 1. A typical EPR signal of Mo(V) in Rh–Mo/ZrO_2 catalyst. The spectrum reported has been recorded from the Mo/Rh = 0.25 sample. Two slightly different species are present: A is probably hexacoordinated Mo(V) and B penta-coordinated.

$g_\perp$ = 1.950, A = 65 G. On the basis of careful analysis of the Mo(V) coordination reported by Louis and Che (23) for Mo/SiO_2, and despite some differences between the perpendicular values it can be inferred that species A is more coordinated than species B. In particular species A should be a hexacoordinated species and species B a pentacoordinated one. By reduction at 523 K the intensity of the signal increases by a factor of two and increases again by the same factor by further reduction at 773 K. A third species (C) with $g_\perp$ = 1.913 (and unresolved $g_\parallel$) appears upon reduction at this latter temperature and is very probably due to four coordinated molybdenum ions: progressive reduction of the sample thus gives rise to less coordinated Mo reduced species.

The EPR signal related to Mo(V) was also observed on the Mo/Rh = 1 sample when outgassed at 523 K. In this case, however, the spectrum was about ten times more intense than the previous one and species A was far more abundant than B. Reduction at 773 K increased the intensity of the spectrum by a factor of two (24, 25).

The Mo(V) signal was present for all the samples even before the reduction *in situ*: increasing the Mo concentration increases the pentacoordinated Mo_{5c}(V) species. Reduction at high temperature favours the formation of the tetracoordinated Mo_{4c}(V). EPR analysis indicates that Mo(V) was present in the passivated sample and its concentration in the samples increases with the temperature of reduction. Generally speaking the increase was proportionately greater in samples with a low molybdenum content. Given the facility with which the redox processes of Mo take place in the presence of Rh, and the possibility for Mo(V) to adopt different states of coordination, it is presumed that molybdenum may be a catalytically active

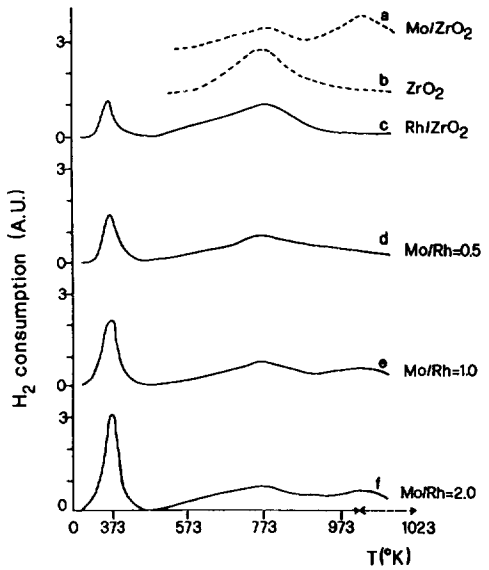

FIG. 2. TPR profiles of the catalysts: (a) Mo/ZrO_2; (b) ZrO_2; (c) Rh/ZrO_2; (d) $Rh–Mo/ZrO_2$ (Mo/Rh = 0.5); (e) $Rh–Mo/ZrO_2$ (Mo/Rh = 1); (f) $Rh–Mo/ZrO_2$ (Mo/Rh = 2).

species, able to bind reversibly molecules such as water and carbon monoxide.

(*c*) *TPR.* The TPR profile (Fig. 2) of the support (ZrO_2) showed a hydrogen consumption peak at about 773 K; the profile of Rh/ZrO_2 catalyst showed a hydrogen consumption peak at about 373 K which was assigned (26) to the reduction of Rh_2O_3, and a broad band at about 773 K, as in ZrO_2 alone. With Mo promoted catalysts two peaks were present, both increasing with the Mo content: the first one at 373 K, without any shift in the maximum temperature T_m, was assigned (26) to the reduction of Rh_2O_3 and a broad one at about 1025 K to the reduction of MoO_3, since the same peak was found in the TPR profile of MoO_3/ZrO_2.

(*d*) *Chemisorption.* In Fig. 3 the chemisorption of hydrogen and oxygen on LTR and HTR catalysts, as a function of the Mo/Rh ratio, is reported. Compared to the LTR treatment, the HTR treatment decreases both the hydrogen and the oxygen chemisorption on the unpromoted catalysts. The addition of Mo decreases the chemisorption of hydrogen while it increases that of oxygen. As already evidenced by EPR results, this behaviour suggests the occurrence of an interaction between Rh and Mo, where the effect of Rh is to favour the formation of Mo bronzes and therefore the increase of oxygen chemisorption. On the other hand, the decoration of Rh particles by reduced MoO_3 decreases H_2 chemisorption.

In Fig. 4 the CO/Rh chemisorption data as a function of the Mo/Rh ratio are reported for LTR catalysts: the

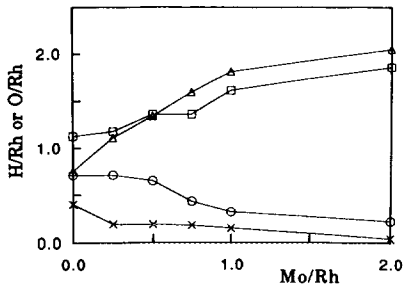

FIG. 3. Oxygen (△, □) and hydrogen (○, ×) chemisorption as a function of Mo/Rh atomic ratio on the LTR (□, ○) and HTR (△, ×) catalysts.

CO/Rh values increased with the Mo/Rh ratio. The amount of chemisorbed CO was lower than expected from H/Rh results on samples with low Mo/Rh ratio, but higher on samples with high Mo/Rh ratio. This suggests that Mo promotes the CO chemisorption on Rh by formation of gem-dicarbonyl species. No significant amounts of CO were chemisorbed on Rh/ZrO_2 HTR catalysts: there was a broad, low-intensity peak revealing the presence of CO adsorbed with a low bond energy, as supported by the observation that CO desorbs even under He stream. On Rh/Mo HTR catalysts the same behaviour was observed, but curiously a two-peak pattern can be seen for Mo/Rh > 0.75 suggesting a possible CO adsorption on some coordinatively unsaturated Mo sites. Chemisorption results and FTIR spectra (see below) showed that MoO_3/ZrO_2 does not adsorb CO.

(*e*) *FTIR spectra.* The spectra of CO adsorbed at saturation (5.32 kPa) on LTR samples are reported in Fig. 5: the Mo/Rh ratio is equal to 0.25 for curve a, 0.75 for curve b, and 2 for curve c. The spectra were normalized to the weight of the wafers and are therefore related to the CO adsorbed per Rh atom at increasing Mo content. In agreement with the literature the band at 2185 cm^{-1} is assigned to CO adsorbed on the Zr^{4+} surface ions of the support (27, 28). The frequency of the linear Rh–CO shifts

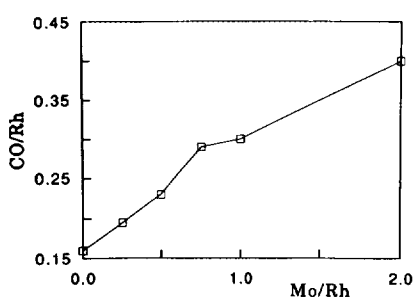

FIG. 4. Carbon monoxide chemisorption on LTR catalysts as a function of the Mo/Rh atomic ratio.

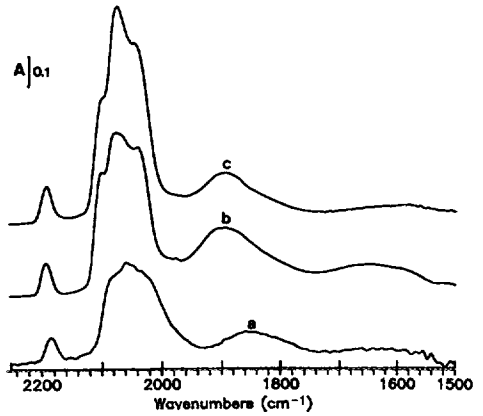

FIG. 5. FTIR spectra of CO adsorbed, at RT and P_{CO} = 5.32 kPa, on Rh–Mo/ZrO_2 catalysts reduced 1 h and outgassed 15 min at 523 K (LTR). All spectra have been normalized to the same total amount of Rh. Curves a, b, and c refer to Mo/Rh ratio = 0.25, 0.75, and 2, respectively.

from 2060 to 2077 cm^{-1} with increasing Mo content. This band was accompanied by two shoulders at 2090–2100 and 2030–2045 cm^{-1}, assigned to $Rh^+(CO)_2$; also the frequency of the bridged Rh_2CO shifts from 1860 to 1900 cm^{-1}, and no other clear components at lower frequencies are observed. A broad, but not well-defined band was present in the 1750–1550 range.

An opposite trend was found for CO adsorbed on HTR samples. The normalized spectra are reported in Fig. 6: going down from curve a (Mo/Rh = 0.5) to curves b (Mo/Rh = 1) and c (Mo/Rh = 2) a strong decrease of the peak intensities is evident. Other relevant features can be observed by making a comparison with LTR spectra: (i) the peak intensity of CO adsorbed on the unsaturated Zr^{4+} sites (29) at 2200–2192 cm^{-1} increases; (ii) the linear CO peak splits into two peaks at 2070 and 2082 cm^{-1} for all the samples and their relative intensity changes with the Mo/Rh ratio (30); (iii) the broad band at 1650 cm^{-1} present in the Mo/Rh = 0.25 sample shifts to frequencies lower than 1600 cm^{-1} and tends to disappear on increasing the Mo content.

As was brilliantly demonstrated by Bredikhin and Lokhov (31) this band must be attributed to a CO bridging a metallic atom and a ZrO_2 site at the metal/support boundary. The considerable width of the band is probably related to the lack of homogeneity of the adsorption centres that are involved.

Figure 7 shows the CO reversibly adsorbed on the HTR sample Mo/Rh = 0.25 from the growth of the spectrum with pressure at RT: curves a–e correspond to the differences between the signal of CO adsorbed at 5.32 kPa and the CO remaining at decreasing values of pressure, until 1.3 10^{-5} kPa. The band at 2200–2192 cm^{-1} is related to

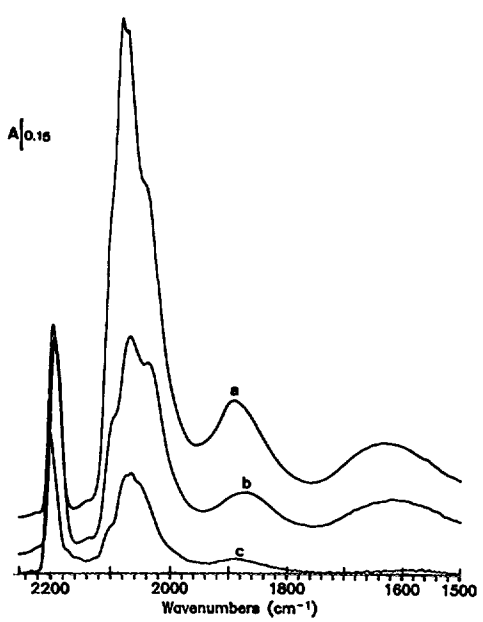

FIG. 6. FTIR spectra of CO adsorbed, at RT and P_{CO} = 5.32 kPa on Rh–Mo/ZrO_2 catalysts reduced 1 h and outgassed 15 min at 773 K (HTR). All spectra have been normalized to the same total amount of Rh. Curves a, b, and c refer to Mo/Rh ratio = 0.50, 1, and 2, respectively.

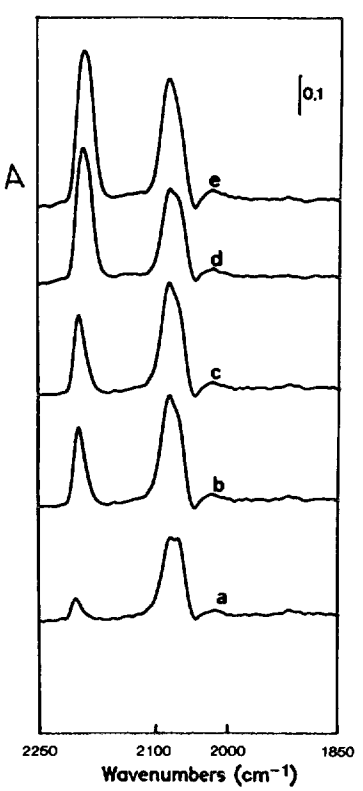

FIG. 7. Difference between the FTIR spectra of CO adsorbed at saturation (5.32 kPa) on Rh–Mo/ZrO_2 catalysts (Mo/Rh = 0.25) and those of CO adsorbed at lower pressure: curves a, b, c, d, and e refer to P_{CO} = 1.73, 0.29, 0.05, 0.013, and 1.3 10^{-5} kPa.

CO adsorbed on Zr^{4+} and totally desorbed at RT. The bands at 2070 and 2082 cm^{-1} (see also Fig. 6) are related to the reversible CO chemisorbed on Rh. This pair of bands was found in all samples: the height of the band at high frequency increased with Mo content. Only one band was normally present in the range 2060–2030 cm^{-1}, assigned to CO bound to Rh^0 (29, 30, 32). The increase of frequency found in our samples can be due to the surface structure of Rh crystallites with unusual high index faces, steps, and kinks. The small negative peak at 2045 cm^{-1} should be noted: it indicates an increase of CO linearly adsorbed on Rh^0, shifted at lower frequency for the decrease of dipole–dipole coupling with the coverage. This analysis shows that by evacuation at RT only the $Rh^+(CO)_2$ and Rh^0CO species remain irreversibly adsorbed.

The reactivity of irreversibly adsorbed CO on the HTR sample Mo/Rh = 1 at 423 and 473 K is presented in Fig. 8. Curve a is the reference spectrum of CO chemisorbed at RT under saturation pressure: in addition to the adsorptions of CO (33) in the range 1800–2100 cm^{-1} (CO on Zr^{4+} and Mo^{4+} at 2181 cm^{-1}; $Rh^+(CO)_2$ at 2100 and 2031 cm^{-1}; $Rh^0(CO)$ at 2057 cm^{-1}; $Rh_2(CO)$ at 1881 cm^{-1}) a broad band at 1630 cm^{-1} is evident. The latter shifts at 1600 cm^{-1} after evacuation at RT (curve b) while the bands of CO adsorbed on Zr^{4+} and Mo^{4+} ions totally disappear (33). After heating the evacuated sample in a closed cell at 423 K, the 1600 cm^{-1} band is further shifted in frequency (curve c), whereas other bands at lower frequencies appear. This spectral picture is demonstrated after further heating at 473 K (curve d), where the band at 1600 cm^{-1} is no longer present. The spectrum is dominated by a band at 2057 cm^{-1}, and by new bands at 1410, 1295 cm^{-1} (carbonates, see Discussion) and at 1560 (sh), 1390 (sh), 1370 cm^{-1} (formates, see Discussion); as a general trend the intensity of the peaks in the range 1880–2100 cm^{-1} are slightly lowered.

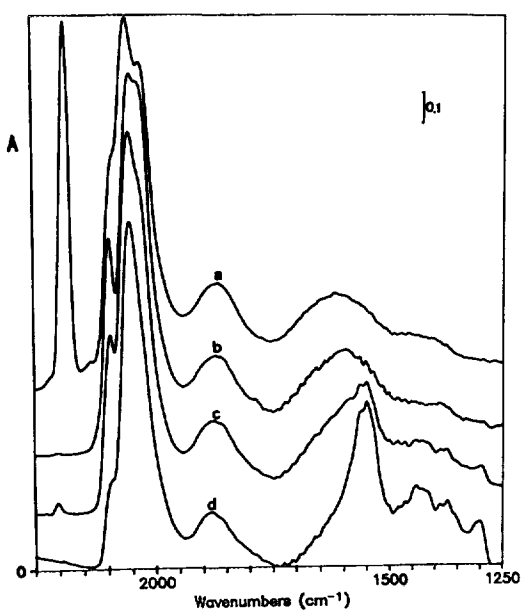

FIG. 8. FTIR spectra of CO adsorbed at increasing temperatures on (HTR) Rh–Mo/ZrO_2 catalyst (Mo/Rh = 1). Curve a: P_{CO} = 5.32 kPa, at room temperature; curve b: sample a after 10 min evacuation; curve c: sample b heated 15 min at 423 K; curve d, sample c heated 15 min at 473 K.

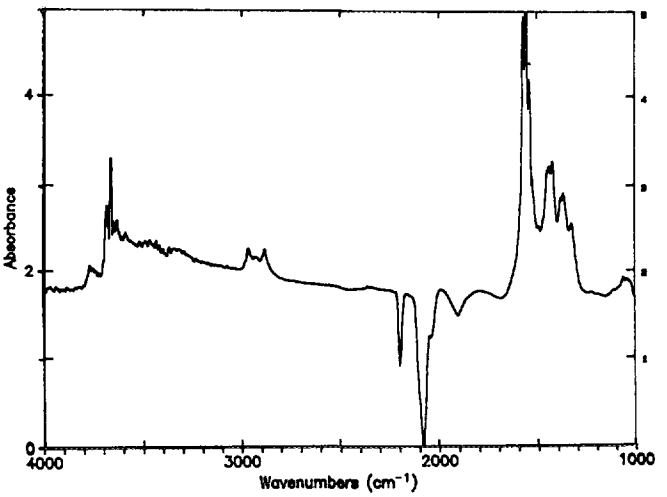

FIG. 9. FTIR spectra difference between the CO spectrum and CO/H_2 spectrum (mixture 1 : 3), heated 20 min at 523 K. Both spectra are recorded at RT under 2.6 kPa on HTR Rh–Mo/ZrO_2 catalysts (Mo/Rh = 0.5).

The reactivity towards CO–H_2 mixture of the Mo/Rh = 0.5 HTR catalyst has been studied. In Fig. 9 is shown the difference between the spectrum taken at RT under a CO/H_2 = 1/3 mixture (total pressure 2.6 kPa) after heating at 523 K for 20 min and the spectrum taken at RT under pure CO (total pressure 2.6 kPa). The negative peaks at 2195, 2076–2038, and 1890 cm^{-1} are due to the CO desorbed from zirconia and to Rh–CO sites consumed by reaction with H_2. The positive peaks refer to the formation of various species: (i) hydroxyl groups and water on zirconia at 3770–3725, 3686, 3663, and 3630 cm^{-1}; (ii) CH_x groups at 2967, 2930, and 2882 cm^{-1}; (iii) formates at 1568, 1380, and 1368 cm^{-1} (27); (iv) bidentate carbonates at 1554–1540, 1325, and 1057 cm^{-1} (34). The bands at 1450–1422 cm^{-1} can be assigned from their intensity both to the CH_x bending modes and to mono/polydentate carbonates formed on the ZrO_2 (34) or the MoO_x phases.

In order to see whether carbon dioxide plays any role in product formation during CO hydrogenation, the CO_2/H_2 reaction was studied. The results are reported in Fig. 10. On the HTR Mo/Rh = 2 sample, the adsorption of pure CO_2 at RT, curve a, produces little CO, shown by the weak band at 2020 cm^{-1} together with bands of linear CO_2 at 2350 cm^{-1} coupled with the symmetric mode at

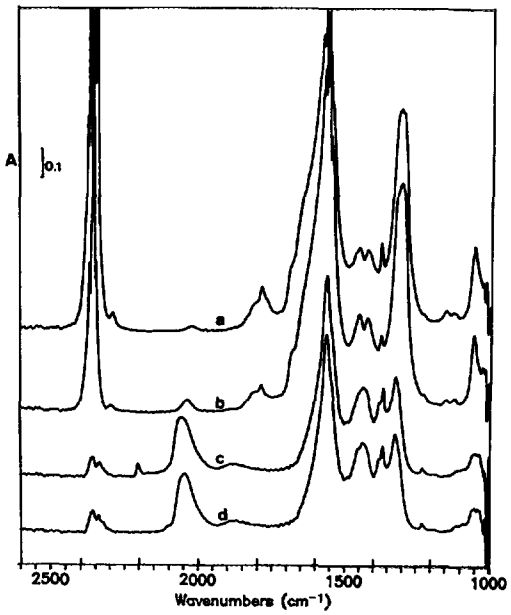

FIG. 10. FTIR spectra of CO_2 adsorbed at RT on a HTR Rh–Mo/ZrO_2 (Mo/Rh = 2). Curve a: P_{CO_2} = 0.66 kPa; curve b: CO_2 evacuated for 5 min and 1 kPa of H_2 added; curve c: after heating 20 min at 523 K; curve d: after 20 min evacuation at RT.

1370 cm^{-1}, both decreasing after evacuation and addition of hydrogen (curves a and b); the formation of formate species by heating at 523 K (curve c) is shown by the bands at 1380–1370 cm^{-1} and by the component at 1560 cm^{-1} together with a carbonate component. In full agreement with the assignments of Bensitel *et al.* (34) for CO_2/ZrO_2, organic-like carbonates appear at 1785–1810 cm^{-1}, bidentate carbonates at 1580–1550 cm^{-1}, 1307 cm^{-1} (broad, shifting to 1320 cm^{-1} at 523 K), and 1055 cm^{-1}, bicarbonates at 1630 (sh), 1450, and 1225 cm^{-1}, and mono/polydentate carbonates at 1425–1410 cm^{-1}. Two weak bands are also formed at 1124 and 1150 cm^{-1} and can be assigned to ethoxy groups (see Discussion). On addition of H_2 (1 kPa) at RT (curve b) the band of CO on Rh^0 increases and slightly shifts to 2034 cm^{-1}. This trend was enhanced by heating at 523 K (curve c): the CO band increased and shifted to 2055 cm^{-1} at the expense of linearly adsorbed CO_2 (2350, 1370 cm^{-1}). A new weak band appeared at 2195 cm^{-1}. The evacuation at RT (curve d) red-shifted the band at 2055 cm^{-1} and eliminated the very weak band at 2195 cm^{-1}, leaving unchanged the other features of the spectrum.

Samples of MoO_3/ZrO_2 (Mo = 1.12 wt. %) activated and reduced in the same conditions as the Rh–Mo/ZrO_2 catalysts (523 and 773 K) showed a CO absorption spectrum quite similar to that found for ZrO_2 alone: a strong and composite band, increasing with the temperature of activation, at 2200–2187 cm^{-1} (CO on coordinatively unsaturated Zr^{4+}) and two weak bands at 2140 and 2115

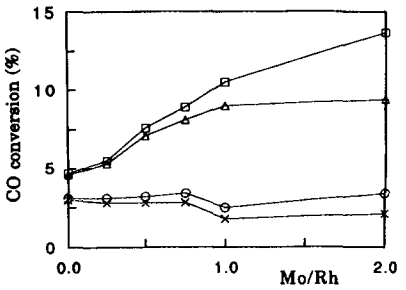

FIG. 11. Total CO conversion (□, ○) and conversion data without the CO conversion to CO_2 (△, ×) as a function of Mo/Rh atomic ratio on LTR (□, △) and HTR (○, ×) catalysts. See text for the experimental conditions.

cm^{-1} as found in the literature (27, 28). Bands due to CO adsorbed on a reduced Mo phase were not found, but it has to be pointed out that surface Mo^{5+}–CO and Mo^{4+}–CO complexes absorb (35, 36) between 2200 and 2180 cm^{-1}, i.e., exactly where Zr^{4+}–CO absorbs.

(*f*) *Catalytic activity.* In Fig. 11 the CO conversion as a function of Mo/Rh atomic ratio is reported for LTR and HTR catalysts. While for LTR catalysts the total CO conversion increased with Mo/Rh ratio, for HTR catalysts the total CO conversion was unaffected. It is important to note that by *increasing the Mo content the amount of CO_2 formed increased significantly*. Figure 11 also shows the conversion of CO to all products other than CO_2: with this correction there is still an increase in CO conversion on LTR catalysts while a small decrease in conversion seems to be present on HTR catalysts.

The CO carbon efficiency to methane and to total hydrocarbons without CO_2 for LTR catalysts was unaffected by the Mo/Rh ratio (Fig. 12) while a constant decrease was observed for HTR-catalysts. In the latter case the decrease in total hydrocarbons must be ascribed mainly to the methane decrease.

On the other hand, the carbon efficiency to ethanol (Fig. 13) differed according to the activation temperature:

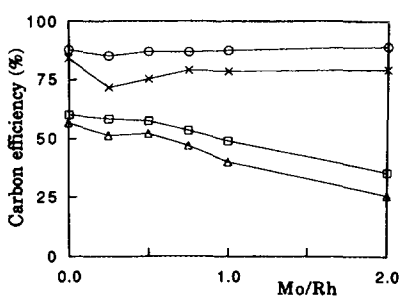

FIG. 12. CO carbon efficiency to total hydrocarbons (○, □) and to methane (×, △) as a function of the Mo/Rh atomic ratio for LTR (○, ×) and HTR (□, △) catalysts.

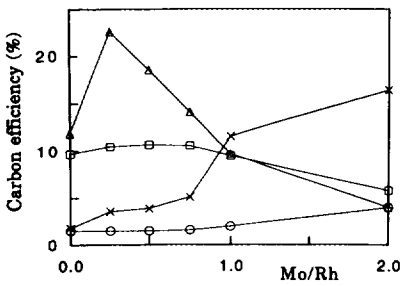

FIG. 13. CO carbon efficiency to methanol (×, ○) and ethanol (□, △) for LTR (□, ○) and HTR (△, ×) catalysts as a function of Mo/Rh atomic ratio.

while on LTR catalysts it decreased very little with the Mo content, on HTR catalysts a significant increase for Mo/Rh = 0.25 occurred, followed by a decrease for higher values. Carbon efficiency to methanol increased with Mo content both on LTR and HTR catalysts, although very mildly in the former case.

As a general consideration the effect of Mo on the activity of Rh/ZrO_2 catalysts strongly depends on the thermal treatment: for low Mo content, high activation temperature favours both methanol and ethanol formation; by increasing the Mo content the CO conversion is increased, mainly due to CO_2 formation.

The most relevant results can be summarized as follows:

(a) activation at high temperature (773 K) diminishes the carbon efficiency of the Rh/ZrO_2 catalyst;

(b) increasing the Mo content increases the carbon efficiency for catalysts activated at low temperature (523 K), whereas for those activated at high temperature it remains practically unchanged;

(c) the addition of Mo promotes the formation of carbon dioxide, especially with catalysts activated at low temperature;

(d) Mo promotes methanol formation especially with catalysts activated at high temperature; if in low concentration, it also promotes ethanol formation.

DISCUSSION

Surface Characteristics

ZrO_2. Monoclinic phase crystals and a minor amount of tetragonal phase crystals, plus probably an amorphous phase, are present in the ZrO_2 used as support. TPR results reveal a slight hydrogen consumption at about 773 K. This may be due either to the formation of Zr^{3+} ions (20), or to a homolytic dissociative chemisorption of hydrogen on dehydrated ZrO_2 with the formation of surface hydroxyl species (37, 38). Although EPR reveals the presence of a signal attributable to the Zr^{3+} ion (but traces of Ti^{3+} or organic radical impurities cannot be excluded), the FTIR spectra suggest that hydrogen chemisorption is the most reliable explanation.

ZrO_2 shows IR absorption bands at 3770, 3725, 3686, 3663, and 3630 cm^{-1} (see, for instance, Fig. 9). In the literature there is agreement on the assignment of the bands at 3780–3760, 3680–3660, and 3400 cm^{-1} to the OH stretching vibrations of Zr(OH), $Zr_2(OH)$, and $Zr_3(OH)$, respectively, on the monoclinic ZrO_2 phase (27, 34, 39), and the band at 3740–3720 cm^{-1} to the stretching vibration of hydroxyl groups on the tetragonal ZrO_2 phase (40). The intensity of the bands at 3770 and 3663 cm^{-1} increases by increasing the pretreatment temperature or the hydrogen adsorption temperature (37, 41). All these hydroxyls are labile and reactive in the sense that they form and can be destroyed very easily (34).

According to Yamaguchi *et al.* (42) the OH species which gives rise to the band at 3780 cm^{-1} is more reactive towards CO than the OH species with a band at 3663 cm^{-1}. Moreover, their acidic properties are lower than those of OH groups on alumina. The IR spectra of chemisorbed carbon monoxide (Fig. 9) display a clear absorption at 2202–2192 cm^{-1} attributed, in agreement with the literature, to CO species formed by interaction with weakly acidic, coordinatively unsaturated (cus) Zr^{4+} (27, 28, 34, 43).

Rh/ZrO_2. Rh is easily oxidized by air to Rh_2O_3 and RhO(OH). EPR spectra of outgassed and reduced samples showed no Rh moieties. TPR results revealed a hydrogen consumption at 373 K attributed to Rh_2O_3 reduction and one at 773 K similar to that on pure ZrO_2.

The effect of thermal treatment is a reduction of both hydrogen and oxygen chemisorption, as previously reported (26), and is attributed to the formation of patches of ZrO_2 on the surface of the Rh particles. During activation under a hydrogen stream, surface hydroxyls are formed with an increase of the ZrO_2 surface mobility which promotes the formation of both patches and surface coordinatively unsaturated Zr^{4+} (cus) species.

FTIR spectra of chemisorbed CO confirm the previous results (29): there are linear and bridged CO species on Rh^0 absorbing at 2060–2040 and 1880 cm^{-1}, a broad, not well-resolved shoulder between 1750 and 1520 cm^{-1}, a range in which there is an absorption band with a maximum at 1650 cm^{-1}, attributed to CO bonded both to Rh particles and ZrO_2. The absorption band of Zr^{4+}–CO at 2202–2192 cm^{-1} is not influenced by the presence of Rh.

Mo/ZrO_2. TPR results revealed consumption of H_2 at 773 K and a second peak at 1000 K assigned to the reduction of MoO_3. CO is not chemisorbed on MoO_3/ZrO_2. This result is confirmed by FTIR results: there was no CO adsorbed on the oxidized or reduced Mo phase, and

the spectrum is similar to that on pure ZrO_2. The intensity of the band at 2202–2192 cm^{-1} does not vary with the molybdenum content in the LTR samples, but is marked with HTR samples and tends to decrease with the molybdenum content. This behaviour is consistent with the fact that the thermal treatment increases the coordinative unsaturation of Zr^{4+}. At the same time, due to a greater mobility at high temperatures, the addition of molybdenum can have a covering action on the Zr^{4+} (cus) ions.

Rh–Mo/ZrO₂. The intense Mo^{5+} EPR signal found after reduction of the samples at 773 K agrees with the formation of a MoO_{3-x} Magnéli phase found by TEM.

The TPR data of Rh–Mo/ZrO_2 (Fig. 2) show a peak of hydrogen consumption corresponding to the reduction of Rh_2O_3 (T = 373 K) and broad peaks at about 773 and 1000 K which could be attributed respectively to the hydrogen adsorbed on ZrO_2 and to the reduction of the MoO_3. The intensity of the signals depends on the Mo content, and this behaviour could appear odd for the peak assigned to the reduction of Rh. In this respect two hypotheses can be put forward: (a) spillover of hydrogen from Rh to MoO_3; (b) reduction of the MoO_3 in contact with the Rh particles.

It is known that even at RT MoO_3 can dissolve atomic hydrogen (44), dissociated by a hydrogen activating metal, with the formation of hydrogen molybdenum bronzes (45). The Rh may act as a hydrogen activator (46). The question is whether the consumption of hydrogen may be due to the formation of molybdenum bronzes or whether the reaction proceeds further to the formation of molybdenum in lower oxidation states.

Both the reduction of pure MoO_3 to MoO_2 and of MoO_2 to Mo metal are catalyzed by low-valent Mo ions (47). The rate-determining step is either H_2 dissociation, when the formation of catalytic sites is limited, or Mo–O bond breaking when an excess of catalytic sites are present. The reduction of MoO_3 depends on the size and the morphology of the sample, on the H_2 partial pressure, on the presence of water, and on the heating rate. MoO_3 may be reduced in the temperature range 625–845 K and MoO_2 at temperatures greater than 845 K (47). When MoO_3 is supported, especially in the presence of hydrogenation catalysts, both reduction temperatures are decreased (47–49). Kip *et al.* (50) hypothesized a reduction of Mo^{6+} to Mo^{2+} upon treatment of Rh/MoO_3 in hydrogen stream at 478 K. Moreover, Bond *et al.* (51–53) showed that in the presence of Pd/SiO_2 a hydrogen molybdenum bronze is formed at RT and this is dehydrated at about 520 K to a lower oxide approximating to Mo_2O_5. In the present case, according to Bond *et al.*, the following reduction scheme for MoO_3 can be proposed:

$$Rh_2O_3/MoO_3 \xrightarrow[H_2]{373\ K} Rh + H_{1.6}MoO_3 + x\,MoO_3 \xrightarrow[H_2]{520\ K} Rh + y\,Mo_2O_5 + 0.8\,H_2O$$

$$H_{1.6}MoO_3 \xrightarrow{298\ K,\ O_2} 0.8\,H_2O + MoO_3 \qquad Mo_2O_5 \xrightarrow{650\ K,\ H_2} Mo_2O_3\ [MoO].$$

SCHEME 1

The chemisorption of hydrogen at 298 K on LTR or HTR catalysts decreases slightly with increase of molybdenum content (Fig. 3), whereas that of oxygen increases markedly (Fig. 3), revealing the presence of reduced molybdenum species easily oxidizable at RT. The chemisorption of carbon monoxide increases with Mo on LTR catalysts, whereas it is more or less negligible on the HTR catalysts.

These data suggest that molybdenum in the HTR catalysts is present as MoO_{3-x}, which results in a constant covering of the Rh particles through the entire Mo/Rh range. This reduces the adsorption of hydrogen on the surface of Rh and inhibits the spillover. The increase in the oxygen chemisorption should be attributed to the oxidation of MoO_{3-x} at the boundary of the Rh particles. To a minor extent the same effects are evident also on LTR catalysts, their extent increasing with the Mo/Rh ratio.

The slight increase in CO chemisorption on LTR catalysts with Mo/Rh atomic ratio (Fig. 4), confirmed also by FTIR data, is in contrast with other reports in the literature. Kip *et al.* (50) and Miura *et al.* (54) observed a decrease in CO adsorption on Rh/Mo/SiO_2 with an increase in the Mo/Rh ratio, paralleled by a decrease in hydrogen chemisorption on catalysts reduced at either 523 or 723 K. These results agree with the low or no hydrogen adsorption at RT on molybdenum in high oxidation states.

We attribute the behaviour of the present catalysts to a different morphology and shape of Rh particles prepared by carbonyl decomposition. The increase of CO chemisorption can be explained by a stronger disruptive and oxidative interaction of the support hydroxyls on the very small Rh particles formed from the Rh carbonyl and inhibited in the sintering by the surrounding MoO_{3-x}, which is also available for CO chemisorption. The formation of gem-dicarbonyl species obviously increases the CO chemisorption.

The addition of a modest amount of molybdenum (Mo/Rh = 0.25) determines a decrease in the intensity of the IR band at 1650 cm^{-1} and in the chemisorption of hydrogen which remains practically constant. For high content of Mo, both LTR and HTR catalysts behave similarly, in agreement with literature data (55).

The oxygen chemisorption is much lower on the unpromoted HTR than LTR catalysts. These results provide further support for the covering effect generated at high temperature by zirconium oxide on Rh particles. The addition of molybdenum promotes oxygen chemisorption: the slope is constant in the LTR catalysts, whereas in the HTR ones a knee is present at Mo/Rh = 1. Quantitative analysis of oxygen chemisorption results on Mo, evaluated from the slope of the lines, are reported in Table 1.

These calculations are based on the assumption that the amount of chemisorbed oxygen on the Rh particles is the same both on the unpromoted and on molybdenum-promoted catalysts, i.e., the degree of decoration of the Rh particles by the zirconium oxide is not influenced by the presence of the molybdenum oxide.

During reduction, the highly dispersed metallic Rh can induce hydrogen spillover and the formation of either molybdenum bronzes or reduced molybdenum oxides. The spillover is particularly evident on LTR catalysts with low molybdenum content (Mo/Rh < 1) while on LTR catalysts with higher molybdenum content (Mo/Rh > 1) a greater amount of molybdenum is present as MoO_3. It seems reasonable to suggest that the high-temperature reduction induces on HTR catalysts with low Mo content (Mo/Rh < 1) a deep MoO_3 reduction with the formation of molybdenum oxides in low oxidation states (MoO_x $x = 1 - 1.5$). This might explain the rapid increase in O_2 chemisorption observed for catalysts with Mo/Rh < 1. On both HTR and LTR catalysts with high molybdenum content (Mo/Rh > 1) the oxygen chemisorbed is the same and is lower than for samples with low Mo content which show an easier MoO_x reducibility.

On all the HTR catalysts, regardless of the molybdenum content, the quantification of the amounts of chemisorbed CO was very difficult owing to the weak and broad profile probably due to a large surface heterogeneity and a low adsorption energy.

TABLE 1

Oxygen Chemisorption on Rh–Mo/ZrO_2 Catalysts: Ratio (Chemisorbed Oxygen Atoms/Mo Atoms) for LTR and HTR Catalysts

	Ratio O/Mo	
Catalyst	LTR	HTR
Mo/Rh <1	0.45	1.05
Mo/Rh >1	0.25	0.25

CO Absorption Bands on Rh–Mo/ZrO_2

The FTIR experiments of CO adsorption on LTR catalysts (Fig. 5) provide indirect evidence of a relation between increased adsorptive capacity and molybdenum content, in agreement with quantitative chemisorption data. The frequencies of CO adsorbed linearly on Rh^0 shift from 2060 (32) to 2077 cm^{-1}, and that of the bridged CO from 1860 to 1900 cm^{-1}. This agrees with the XPS results of Foley *et al.* (55) which show, for a Rh–Mo/Al_2O_3 system, the presence of slightly electropositive Rh centres formed by the interaction of MoO_3 with a highly dispersed Rh. The higher values found in our Rh/Mo samples (2082–2070 cm^{-1}) favour the hypothesis of highly dispersed Rh particles, slightly electropositive due to MoO_3 texture effects, with an increase of the adsorbed CO frequency.

Otherwise, as previously discussed in part (e) of the Results section, the presence in our samples of Rh high index faces, steps, and kinks can simply explain the high frequency shift of CO adsorbed on Rh^0. The observed two bands at 2082–2070 cm^{-1} (Fig. 7) can therefore be assigned to CO reversibly adsorbed on particular Rh^0 sites made slightly electropositive by Mo_xO_y covering the Rh moieties. Similar conclusions have been proposed by Wardinsky and Hecker (30) for Rh/MoO_3 supported on silica. We cannot however exclude the assignments of these bands to $Rh^+ \ldots CO$, but our data do not allow us to make a choice between these possibilities.

The presence on the samples activated at 523 or at 773 K (Figs. 5 and 6) of $Rh^+(CO)_2$ surface groups with bands at 2090–2100 and 2030–2045 cm^{-1} (56) is due to the oxidative interaction of the surface hydroxyls of the support with Rh. The difficulty in reducing the Rh^+ species with H_2 even at 773 K is due to the stability of the surface hydroxyls of zirconia at this temperature (27). In HTR samples the decrease in CO adsorption capacity with the increase of MoO_3 content agrees with the IR data for Rh–MoO_3/SiO_2 (50). The possible formation of Mo^{5+} sites (weak CO absorption at 2200 cm^{-1}) cannot be detected because of the Zr^{4+}–CO band at 2185 cm^{-1}. The presence of more reduced Mo sites, such as Mo^{4+} (2175 cm^{-1}), Mo^{2+} (2140–2080 cm^{-1}), and Mo^0 (2000 cm^{-1}), cannot be proved here (33).

The decrease in the Rh surface exposed to CO at 773 K (Fig. 6) agrees with the simple MoO_3 coating model proposed in the literature (50).

The experiments presented in Fig. 8 are particularly relevant. They show the following:

(a) After evacuation and heating at 473 K Rh^0–CO species at 2057 cm^{-1} and $(Rh^0)_2$–CO species at 1896 cm^{-1} are

particularly stable, while Rh^0–CO and Rh^+–$(CO)_2$ decrease and tend to disappear. Comparison of the b and c curves shows that the heating at 423 K breaks some weak Rh–CO bonds and restores the Zr^{4+}–CO bonds.

(b) The metal/support boundary CO band at 1650–1600 cm^{-1}, with no partner band at lower frequencies, shifts to a lower frequency and changes shape (curve d) with formation of carbonate bands (34) at 1550–1295 cm^{-1} on ZrO_2.

Two types of carbon monoxide bond at the metal/support boundary have been proposed (31, 57):

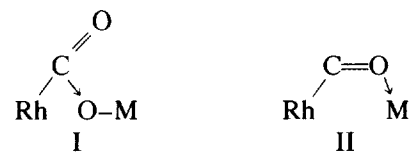

[2]

Both complexes are known from coordination chemistry in solution: type I complex, which is formally analogous to a carboxylate (RCOOM) complex with Rh instead of R, should have bands near 1745 cm^{-1} and 1200 cm^{-1} (58, 59), not found in the present FTIR spectra.

According to Bredikhin and Lokhov (31) and Knözinger (60) type II has quite a low ν(CO) frequency, often below 1700 cm^{-1} as we found. Nevertheless, as suggested by coordination chemistry in solution, type II requires the presence of strong Lewis acid centers, but, as shown above, the ZrO_2 used here has a very low surface acidity so the surface concentration of type II CO must be rather low.

Two other weak bands at 1435–1410 cm^{-1} which have never been seen by adsorption of CO on pure ZrO_2 can be assigned to monodentate carbonate (34), stable up to high temperature (61–63). The presence of monodentate carbonate can be explained only through the dissociation of carbon monoxide followed by the formation of carbon dioxide.

Surface Reactivity of CO/H_2 and CO_2/H_2 on Rh–Mo/ZrO_2

The experiments on the H_2–CO reaction carried out at 523 K (Fig. 9) clearly show that new species are formed at the expense of the reacted CO (negative IR bands at 2195, 2076–2038, and 1890 cm^{-1}). Hydroxyl groups and water are formed (absorbing at 3770–3630 cm^{-1}, as found on ZrO_2) and react with CO, mainly producing formate species on the surface. This result agrees with experiments on ZrO_2 alone (27, 35). The band at 2930 cm^{-1} can be assigned to the CH_3 stretching of a methoxy group (27), formed by formate hydrogenation.

The reduction of CO_2 on Rh/SiO_2 catalysts and on Rh single crystals (64) is already effective in H_2 atmosphere at RT. Figure 10, curve a, shows that small amounts of CO_2, without hydrogen, can be decomposed to CO. Furthermore, together with linear CO_2 at 2350 cm^{-1}, other species such as different types of carbonates and formates are formed, as previously discussed. The bands at 1450–1410 cm^{-1} have been assigned to monodentate carbonate species and/or to the δ_{CH} mode of some alcoholate species adsorbed on ZrO_2, together with the weak bands at 1150–1124 cm^{-1} (65). Curve b shows that some of the above-mentioned species are reduced to CO at RT in the presence of hydrogen. With dipole–dipole coupling on metals the band of CO on Rh^0 shifts from 2020 to 2034 cm^{-1} and further to 2055 cm^{-1} for an increasing coverage near saturation (curve c). The weak band at 2195 cm^{-1} proves that Zr^{4+} sites begin to be populated by CO. For the same dipole coupling effect the 2055-cm^{-1} band red-shifts to 2043 cm^{-1} by evacuation at RT (curve d).

Curve c shows that most of the CO is formed at 523 K with a strong lowering of the carbonate and formate species which seem to be the intermediates in the CO_2 reduction.

Reaction Mechanism

CO_2 formation and reduction. The present work has shown that although the activity of LTR catalysts is higher than that of HTR catalysts the amount of CO converted to CO_2 is the same for both, changing from 3% for Rh/ZrO_2 to 34% for Rh–Mo/ZrO_2 with Mo/Rh = 2. Bhore *et al.* (48) report that the addition of Mo to Rh catalysts on different supports significantly increases the production of CO_2.

Marengo *et al.* (2) have shown that, with catalysts similar to those used in the present study, under CO stream the formation of carbon dioxide begins at temperatures lower than 400 K and changes linearly with the temperature in the case of catalysts unpromoted with molybdenum, whilst there is a sharp increase at about 420–430 K with molybdenum-promoted catalysts.

The CO_2 formation could be the key to the study of promoted catalysts, as molybdenum markedly affects the carbon efficiency of the process. Knowledge of the CO_2-formation mechanism can be useful to clarify not only the role of molybdenum in the early steps of the process, but also the role of CO_2 in the reaction path.

CO_2 formation can occur according to the Boudouard reaction or the water–gas shift reaction. The Boudouard reaction may take place through a CO dissociation according to the scheme:

$$\begin{aligned} CO + 2\sigma &\longrightarrow C(\sigma) + O(\sigma) \\ CO + O(\sigma) &\longrightarrow CO_2 + \sigma, \end{aligned} \qquad [3]$$

where σ is a surface site active in CO dissociation. In the latter reaction, CO can be either adsorbed or in the gas-

eous phase. According to Klier (66) the activation energy necessary to break the CO bond would be such that this process appears most improbable.

Another possible reaction path is the disproportionation

$$2CO \longrightarrow CO_2 + C, \qquad [4]$$

which implies the simultaneous breaking and formation of a carbon–oxygen bond.

Some authors assert that CO desorbs from Rh (either single crystal (67) or polycrystalline (17)), without dissociation until 550 K. Other authors have shown that on Rh surfaces showing irregularities (steps, kinks, defects) and heated to 675 K, both CO desorption and dissociation occur (16); however, at the same time there is no formation of CO_2 because at temperatures higher than 400 K oxygen starts to diffuse within the metallic Rh (68, 69) at a rate faster than that of either the recombination with residual C present on the surface or the reaction with adsorbed CO. Solymosi and Erdöhelyi (70) observed the dissociation of CO on highly dispersed Rh at temperatures above 473 K.

In the case of shift reactions there is agreement that the reactions pass through the formation of a formate species according to the scheme

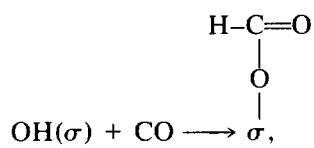

[5]

where OH(σ) is a hydroxyl group on the ZrO_2 surface.

It has been reported that on ZrO_2 the formate species forms through the reduction of a species of bidentate bicarbonate that in its turn is formed by reaction between CO and surface hydroxyl groups (71).

The next stage is the breaking of the C–H bond through an active center which has a great affinity for hydrogen (72). According to Solymosi *et al.* (73, 74) formate spilt over onto the support may decompose through two possible reaction pathways:

$$HCOO(\sigma) \rightleftharpoons CO_2 + H(\sigma) \qquad [6]$$

$$HCOO(\sigma) + n\sigma \longrightarrow H(\sigma) + CO(\sigma) + O(\sigma). \qquad [7]$$

The former is favoured at high and the latter at low formic acid coverage.

Our experimental results have confirmed that ZrO_2 easily adsorbs hydrogen with the formation of various reactive hydroxyl species. Furthermore He and Ekerdt (75) have shown that on ZrO_2 pretreated with oxygen or hydrogen at 593 K, CO_2 can be formed in the temperature range 393–453 K, and have suggested that the precursor could be a bicarbonate species according to Solymosi *et al.* (74).

On the basis of the experimental results we suggest that CO_2 formation in the absence of hydrogen can take place according to the Boudouard reaction through a dual site dissociation mechanism that involves metallic and oxophilic sites of the support according to the scheme

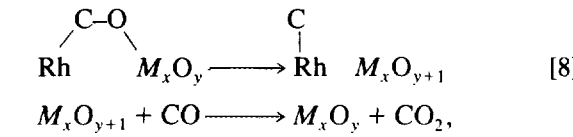

[8]

$$M_xO_{y+1} + CO \longrightarrow M_xO_y + CO_2,$$

where M generically indicates a surface cation. The ZrO_2 has weak oxophilic properties essentially associated with the surface coordinative unsaturation of the ZrO_2 at the boundary of the Rh particle. The molybdenum, present in the reduced form, has superior oxophilic properties that involve coordinatively unsaturated Mo^{5+}. The Zr and Mo sites operate at the same time but due to the different activation energies, lower on ZrO_2, any increase in temperature favours reaction on Mo^{5+}.

In the presence of hydrogen the mechanism may be different: from FTIR results (Fig. 9) it seems that ZrO_2 becomes saturated by hydrogen, either by direct reaction or by spillover, with the formation of surface OH groups. It would be reasonable to assume the same also for molybdenum oxides.

On this basis we suggest that the CO_2-formation mechanism goes through surface formate species according to:

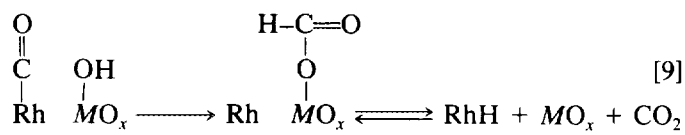

[9]

$$RhH + MO_x + H_2O \longrightarrow Rh + M(OH)O_x + H_2. \qquad [10]$$

On heating at 425 K it can be seen (Fig. 8) that the CO groups bridge the Rh and a cation of the support, evolving towards the formation of bidentate carbonates, whilst in the presence of hydrogen (Fig. 9) there is the definite formation of a formate species. As already stated, the bidentate carbonate species cannot be considered to be the precursor of the formate species as the carbonates are very stable to both thermal and reducing treatments.

The formate species is reactive (Fig. 10) and could be the precursor of many chemical species inasmuch as dehydrogenation is not the only possible reaction.

Methanol formation. While the mechanism of methanol formation on metallic oxides appears to have been clarified (7), the question is still open on supported metals.

Evidence in the literature excludes a dissociative mechanism of CO not only with oxides but also with supported metals (76, 77).

Jackson and Ekerdt (78) have studied the formation of methanol on pure zirconia and concluded that water was required to produce methanol, and also that none of the oxygen from water was incorporated into methanol. In that work there remains some ambiguity concerning the formation of methanol at a temperature of 398 K (75) and the participation of a large amount of lattice oxygen in methanol formation and the dissociative adsorption of water on the Zr cations producing linear and bridged hydroxyl groups (39, 79). However, Jackson and Ekerdt's scheme II, proposed on the basis of a hydrogenation mechanism of CO to methanol in homogeneous phase (80), has several points in common with other mechanisms proposed for the formation of methanol on metals.

In accordance with FTIR results and with other data in the literature it is our opinion that the active species for the formation of methanol is a CO bonded along the boundary of the Rh metal particles and a cation of the support (1650-cm^{-1} band). This band evolves rapidly with heating in H_2, as has already been discussed, with the formation not only of the above-mentioned formate species but also of other species, among which are the CH_x (bands in the 2880–2970 cm^{-1} region) and methoxyl groups (around 1000–1050 cm^{-1}), although more correctly it must be pointed out that, given the complexity of the spectrum, the assignment of the bands is uncertain. The mechanism we propose is:

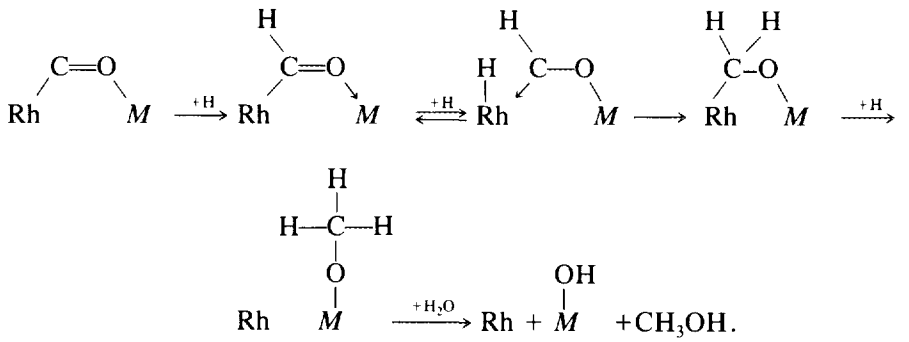

[11]

Intermediate species such as formyl or oxymethylene are highly reactive and rapidly evolve to methoxy. The determining role of water in the last stage was suggested by Klier (66) on the basis of thermodynamic considerations which indicate that the hydrolysis of the methoxy group is energetically favoured with respect to methanol hydrogenation, implying the breaking of the *M*–O bond. However, a possible hydrogenation of oxymethylene group with C–O bond breaking and methane formation cannot be excluded. The facility with which the coordinatively unsaturated cations Mo^{5+} can associate water molecules (23) can explain the increase in methanol formation with catalysts promoted with Mo. Furthermore, it should be noted that the formation of the *M*OH species formed with methanol, can promote the formation of the formate species.

Methane formation. The possible mechanisms for the formation of methane are many. They range from the dissociation of CO followed by hydrogenation of surface carbon atoms to the direct hydrogenation of the CO adsorbed on Rh with the formation of formyl, hydroxycarbene, carbene groups, and others.

Research carried out on the hydrogenation of CO_2 with catalysts (2) similar to those used in the present work has shown that increasing the CO_2 content in the $CO+H_2$ mixture produces a continuous increase in methane. Methanol initially increases until the CO_2 content reaches 8–10% but decreases for higher values. Ethanol follows the course of methanol but decreases (Fig. 13) to a greater extent. From these data it can be seen that high values of CO_2 favour the formation of methane. Schild *et al.* (62) showed with FTIR techniques that on Pd/ZrO_2 catalysts the CO_2 in the presence of hydrogen forms surface methoxy, formyl, and formate species, the latter evolving to methane. One possible way of methane formation can be through CO_2 according to the following mechanism:

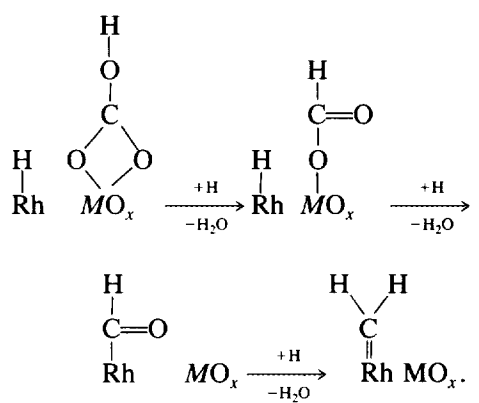

[12]

Actually the monodentate or bidentate bicarbonate species may be hydrogenated to formate (75). This formate

may decompose to CO and H_2O or be reduced to a very unstable Rh-formyl intermediate that is hydrogenated to a carbenic species, the effective precursor in the hydrogenation to methane.

For low surface concentrations the formate species tend to decompose with the formation of CO and H_2O, whilst at high concentrations they tend to dehydrogenate with the formation of carbon dioxide. In the presence of a great excess of carbon dioxide, or else when the adsorption of hydrogen on Rh is not hindered by the presence of carbon monoxide, the reduction of the formate to carbenic species, through a formyl intermediate, can take place.

ACKNOWLEDGMENTS

Financial support from CNR (Rome), P. F. Chimica Fine e Secondaria, and MURST (Rome) is gratefully acknowledged.

REFERENCES

1. Bhasin, M. M., Bartley, W. J., Ellgen, P. C., and Wilson, T. P., *J. Catal.* **54,** 120 (1978).
2. Marengo, S., Martinengo, S., and Zanderighi, L., *Chem. Eng. Sci.* **47,** 2793 (1992).
3. Underwood, R. P., and Bell, A. T., *Appl. Catal.* **21,** 157 (1986).
4. Kiennemann, A., Breault, R., Hindermann, J. P., and Laurin, M., *J. Chem. Soc. Faraday Trans.* **83,** 2119 (1987).
5. Ponec, V., *Catal. Today* **12,** 227 (1992).
6. Sachtler, W. M. H., and Ichikawa, M., *J. Phys. Chem.* **90,** 4752 (1986).
7. Chinchen, G. C., Mansfield, K., and Spencer M. S., *CHEMTECH* **20,** 692 (1990).
8. Bell, A. T., *Catal. Rev.—Sci. Eng.* **29,** 203 (1981).
9. Orita, H., Naito, S., and Tamaru, K., *J. Catal.* **90,** 183 (1984).
10. Jackson S. D., Brandreth, B. J., and Winstanley, D., *J. Catal.* **106,** 464 (1987).
11. Ellgen, P. C., Bartley, W. J., Bhasin, M. M., and Wilson, T. P., *Adv. Chem. Ser.* **178,** 147 (1979).
12. Ichikawa, M., *CHEMTECH* **12,** 674 (1982).
13. Ponec, V., and Nonneman, L. E. Y., *Stud. Surf. Sci. Catal.* **61,** 225 (1991)
14. Koerts, T., and van Santen, R. A., *J. Catal.* **134,** 13 (1992).
15. Burch, R., and Petch, M. I., *Appl. Catal. A* **88,** 61 (1992).
16. Castner, P., and Somorjai, G. A., *Surf. Sci.* **83,** 60 (1979); ibid **103,** L134 (1981).
17. Gorodetskii, V. V., Nieuwenhuys, B., *Surf. Sci.* **105,** 299 (1981).
18. Castner, D. G., Blackadar, R. L., and Somorjai, G. A., *J. Catal.* **66,** 257 (1980).
19. Marengo, S., Miessner, H., Trunschke, A., Martinengo, S., and Zanderighi, L., *Collect. Czech. Commun.* **57,** 2565 (1992).
20. Morterra, C., Giamello, E., Orio, L., and Volante, M., *J. Phys. Chem.* **94,** 3111 (1990).
21. Shelimov, B. N., Pershin, A. N., and Kazansky, V. B., *J. Catal.* **64,** 426 (1980).
22. Che, M., McAteer, J., and Tench, A. J., *J. Chem. Soc., Faraday Trans. 1* **74,** 2378 (1978).
23. Louis, C., and Che, M., *J. Phys. Chem.* **91,** 2875 (1987).
24. Guglielminotti, E., and Giamello, E., *J. Chem. Soc., Faraday Trans. 1* **81,** 2307 (1985).
25. Garrone, E., and Stone, F. S., *in* "Proceedings, 8th International Congress on Catalysis, Berlin, 1984," Vol. 3, p. 441. Dechema Frankfurt-am-Main, 1984.
26. Dall'Agnol, C., Gervasini, A., Morazzoni, F., Pinna, F., Strukul, G., and Zanderighi, L., *J. Catal.* **96,** 106 (1985).
27. Guglieminotti, E., *Langmuir* **6,** 1455 (1990).
28. Bolis, V., Morterra, C., Volante, M., Orio, L., and Fubini, N., *Langmuir* **6,** 695 (1990).
29. Guglielminotti, E., *J. Catal.* **120,** 287 (1989).
30. Wardinsky, M. D., and Hecker, W. C., *J. Phys. Chem.* **92,** 2602 (1988).
31. Bredikhin, M. N., and Lokhov, Yu. A., *Kinet. Katal.* **28,** 591, 678 (1987).
32. Dubois, L. H., and Somorjai G. A., *Surf. Sci.* **91,** 514 (1980).
33. DeCanio, E. C., and Storm, D. A., *J. Catal.* **132,** 375 (1991).
34. Bensitel, M., Saur, O., and Lavalley, J. C., *Mater. Chem. Phys.* **17,** 149 (1987).
35. Peri, J. B., *J. Phys. Chem.* **86,** 1615 (1982).
36. Zaki, M. I., Vielhaber, B., and Knözinger, H., *J. Phys. Chem.* **90,** 3183 (1986).
37. Onishi, T., Abe, H., Maruya, K., and Domen, K., *J. Chem. Soc., Chem. Commun.*, 617 (1985).
38. Kondo, J., Sakata, Y., Domen, K., Maruya, K.-I., and Onishi, T., *J. Chem. Soc., Faraday Trans.* **86,** 397 (1990).
39. Tret'yakov, N. E., Pozdnyakov, D. V., Oranskaya, O. M., and Filimonov, V. N., *Russ. J. Phys. Chem. (Engl. Transl.)* **44,** 596 (1970).
40. Hertl, W., *Langmuir* **5,** 96 (1989).
41. Kondo, J., Abe, H., Sakata, Y., Maruya, K., Domen, K., and Onishi, T., *J. Chem. Soc., Faraday Trans. 1* **84,** 511 (1988).
42. Yamaguchi, T., Nakano, Y., and Tanabe, K., *Bull. Chem. Soc. Japan* **51,** 2482 (1978).
43. Onishi, T., Maruya, K., Domen, K., Abe, H., and Kondo, J., *in* "Proceedings, 9th International Congress on Catalysis, Calgary, 1988" (M. J. Phillips and M. Ternan, Eds.). Vol. 2, p. 507. Chem. Institute of Canada, Ottawa, 1988.
44. Hegedus, A. J., Sasvari, K., and Neugebauer, J., *Z. Anorg. Allg. Chem.* **293,** 56 (1957).
45. Fripiat, J. J., *in* "Surface Properties and Catalysis by Non-Metals" (J. P. Bonnelle, B. Delmon, and E. Derouane, Eds.), p. 477. Reidel Pu. Co, Dordrecht, 1983.
46. Sermon, P. A., and Bond, G. C., *Catal. Rev.* **8,** 221 (1973).
47. Arnoldy, P., de Jonge, J. C. M., and Moulijn, J. A., *J. Phys. Chem.* **89,** 4517 (1985).
48. Bhore, N. A., Sudhaker, C., Bischoff, K. B., Manogue, W. H., and Mills, G. A., *in* "Proceedings, 9th International Congress on Catalysis, Calgary, 1988" (M. J. Phillips and M. Ternan, Eds.), Vol. 2, p. 594. Chem. Institute of Canada, Ottawa, 1988.
49. Van den Berg, F. G. A., Glezer, J. H. E., and Sachtler, W. M. H., *J. Catal.* **93,** 340 (1985).
50. Kip, B. J., Hermans, E. G. F., van Wolput, J. H. M. C., Hermans, N. M. A., van Grondelle, J., and Prins, R., *Appl. Catal.* **35,** 109 (1987).
51. Bond, G. C., and Tripathi, J. B. P., *J. Less-Common Met.* **36,** 31 (1974).
52. Bond, G. C., and Sermon, P. A., *J. Chem. Soc., Faraday Trans. 1* **72,** 730 (1976).
53. Bond, G. C., and Tripathi, J. B. P., "Chemical Uses of Molybdenum, Proc. 1st Conf., 1973," p. 17. Mitchell P. C. H., Climax Molybdenum Co., London, 1974.
54. Miura, H., Osawa, M., Sugiyama, K., and Matsuda, T., *J. Catal.* **101,** 178 (1986).
55. Foley, H. C., Hong, A. J., Brinen, J. S., Allard, L. F., and Garrat-Reed, A. J., *Appl. Catal.* **61,** 351 (1990).
56. Ballinger, T. H., and Yates, J. T., *J. Phys. Chem.* **95,** 1694 (1991).

57. Lavalley, J. C., Saussey, J., and Lamotte, J., *J. Phys. Chem.* **94,** 5941 (1990).
58. Gambarotta, S., Floriani, C., Chiesi-Villa, A., and Guastini, C., *J. Am. Chem. Soc.* **107,** 2985 (1985).
59. Aresta, M., and Nobile, C. F., *J. Chem. Soc., Dalton Trans.,* 708 (1977).
60. Knözinger, H., *in* "Proceedings of the 5th International Symposium on Relation between Homogeneous and Heterogeneous Catalysis, Novosibirsk, 1986" (Yu. Yermakov and V. Likholobov, Eds.), p. 789. VNU Science Press, Utrecht, 1986.
61. Kiselev, V. F., and Krylov, O. V., "Adsorption and Catalysis on Transition Metals and Their Oxides." Springer, Berlin, 1989.
62. Schild, C., Wokaun, A., and Baiker, A., *J. Mol. Catal.* **63,** 223 (1990).
63. Li, C., Sakata, Y., Arai, T., Domen, K., Maruya, K., and Onishi, T., *J. Chem. Soc., Faraday Trans. 1,* **85,** 929 (1989).
64. Solymosi, F., and Knözinger H., *J. Catal.* **122,** 166 (1990).
65. Hussein, G. M. A., Sheppard, N., Zaki, M. I., and Fahin, R. B., *J. Chem. Soc., Faraday Trans.* **87,** 2655, (1991); ibid **87,** 2661 (1991).
66. Klier, K., *Adv. Catal.* **31,** 243 (1982).
67. Yates, J. T., Williams, E. D., and Weinberg, W. H., *Surf. Sci.* **91,** 562 (1981).
68. Thiel, P. A., Williams, E. D., Yates, J. T., and Weinberg, W. H., *Surf. Sci.* **84,** 54 (1979).
69. Thiel, P. A., Yates, J. T., and Weinberg, W. H., *Surf. Sci.* **82,** 22 (1972).
70. Solymosi, F., and Erdöhelyi, A., *Surf. Sci.* **110,** L630 (1981).
71. Silver, R. G., Jackson, N. B., and Ekerdt, J. G., *in* "Catalytic Activation of Carbon Dioxide," p. 123. American Chem. Soc., Washington, 1988.
72. Mars, P., Scholten, J. J. F., and Zwietering, P., *Adv. Catal.* **14,** 35 (1963).
73. Solymosi, F., Kiss, J., and Kovacs, I., *Surf. Sci.* **192,** 47 (1987).
74. Solymosi, F., Erdöhelyi, A., and Bánsági, T., *J. Chem. Soc., Faraday Trans. 1* **77,** 2645 (1981).
75. He, M. Y., and Ekerdt, J. G., *J. Catal.* **90,** 17 (1984); ibid **87,** 381 (1984).
76. Rabo, J. A., Risch, A. P., and Poutsma, M. L., *J. Catal.* **53,** 295 (1978).
77. Takeuchi, A., and Katzer, J. R., *J. Phys. Chem.* **85,** 937 (1981).
78. Jackson, N. B., and Ekerdt, J. G., *J. Catal.* **101,** 90 (1986).
79. Agron, P. A., Fuller, E. L., and Holmes, H. F., *J. Colloid Interface Sci.* **52,** 553 (1975).
80. Marinquez, J. M., McAlister, D. R., Sanner, R. D., and Bercaw, J. E., *J. Am. Chem. Soc.* **100,** 2716 (1978).